



Hygro-thermo-chemical modeling of high-performance concrete. II: Numerical implementation, calibration, and validation

Giovanni Di Luzio^a, Gianluca Cusatis^{b,*}

^a Department of Structural Engineering, Politecnico di Milano, Milan, Italy

^b Department of Civil and Environmental Engineering, 4048 Johnson Engineering Center, Rensselaer Polytechnic Institute, 110 Eighth St, Troy, NY 12180-3590, USA

ARTICLE INFO

Article history:

Received 12 September 2008

Received in revised form 19 February 2009

Accepted 25 February 2009

Available online 13 March 2009

Keywords:

Concrete

Early age

Moisture

Temperature

Relative humidity

Hydration

Silica fume

Self-desiccation

ABSTRACT

This paper presents the numerical implementation, calibration, and validation of the hygro-thermo-chemical model formulated theoretically in the companion paper [Di Luzio G, Cusatis G. Hygro-thermo-chemical modeling of high-performance concrete. I: Theory. *Cem Concr Compos*, in press, doi:10.1016/j.cemconcomp.2009.02.015.]. Calibration and validation are based on experimental data gathered from the literature and relevant to hydration, self-desiccation, and drying of standard and high-performance concrete with and without silica fume.

© 2009 Elsevier Ltd. All rights reserved.

1. Introduction

In the companion paper (Part I of this study) [1], a new model for moisture transport and heat transfer in high-performance concrete (HPC) has been formulated. This model accounts for the effect of cement hydration, silica fume (SF) reaction, and silicate polymerization on early age and long-term aging of HPC, by formulating a theoretical framework where the kinetics of the chemical reactions is described by Arrhenius-type evolution laws. This makes it possible to simulate self-heating, self-desiccation and drying from the very early age in a thermodynamically consistent fashion. In the present Part II, the numerical implementation of the model is presented and the model is calibrated and validated by analyzing experimental data gathered from the literature. A wide range of typical experimental tests, including desorption tests, isothermal and adiabatic calorimetric tests, self-desiccation tests, and drying tests, are numerically simulated in order to check accuracy and predictive capability of the proposed formulation. All the definitions and notations introduced in the companion paper are retained hereinafter.

2. Numerical implementation

As discussed in the companion paper [1], moisture transport and heat transfer in high-performance concrete can be modeled

by two partial differential equations (governing mass and energy conservation at the macroscopic level) coupled with three evolution laws for hydration degree, silica fume reaction degree, and concentration of silicate polymers (all treated as internal variables).

In an axis-symmetric setting, the mass and energy conservation laws (Eqs. (4) and (11) in [1]) can be rewritten as

$$\frac{\partial}{\partial r} \left(D_h \frac{\partial h}{\partial r} \right) + \frac{D_h}{r} \frac{\partial h}{\partial r} + \frac{\partial}{\partial z} \left(D_h \frac{\partial h}{\partial z} \right) + C_1 \frac{\partial h}{\partial t} + C_2 = 0 \quad (1)$$

$$\frac{\partial}{\partial r} \left(\lambda \frac{\partial T}{\partial r} \right) + \frac{\lambda}{r} \frac{\partial T}{\partial r} + \frac{\partial}{\partial z} \left(\lambda \frac{\partial T}{\partial z} \right) + C_3 \frac{\partial T}{\partial t} + C_4 = 0 \quad (2)$$

where $C_1 = -\partial w_e / \partial h$, $C_2 = -F_h(h, \alpha_c, \alpha_s, \alpha_p)$, $C_3 = -\rho c_t$, and $C_4 = F_t(\alpha_c, \alpha_s)$.

By using the classical Galerkin [2] method based on the use of the weak formulation of the differential problem and a finite element approximation of the primary variables, $h(r, z, t) \approx \sum_i^N h_i(t) N_i(r, z)$, $T(r, z, t) \approx \sum_i^N T_i(t) N_i(r, z)$ ($N_i(r, z)$ = shape functions, N = number of element nodes), one obtains

$$\mathbf{K}_1 \dot{\mathbf{h}} + \mathbf{K}_2 \mathbf{h} + \mathbf{F}_1 = \mathbf{0} \quad (3)$$

$$\mathbf{K}_3 \dot{\mathbf{T}} + \mathbf{K}_4 \mathbf{T} + \mathbf{F}_2 = \mathbf{0} \quad (4)$$

where the matrices \mathbf{K}_1 , \mathbf{K}_2 , \mathbf{K}_3 , \mathbf{K}_4 , and the vectors \mathbf{F}_1 , \mathbf{F}_2 are obtained by the global assemblage of element level matrices given by

* Corresponding author. Tel.: +1 518 276 3956; fax: +1 518 276 4833.
E-mail addresses: cusat@rpi.edu, giacusatis@yahoo.it (G. Cusatis).

$$K_{1,ij}^{ele} = \int_{ele} C_1 N_i N_j d\Omega$$

$$K_{2,ij}^{ele} = \int_{ele} \left[D_h \left(-\frac{\partial N_i}{\partial r} \frac{\partial N_j}{\partial r} + \frac{N_j}{r} \frac{\partial N_i}{\partial r} - \frac{\partial N_i}{\partial z} \frac{\partial N_j}{\partial z} \right) \right] d\Omega \quad (5)$$

$$K_{3,ij}^{ele} = \int_{ele} C_3 N_i N_j d\Omega$$

$$K_{4,ij}^{ele} = \int_{ele} \left[\lambda \left(-\frac{\partial N_i}{\partial r} \frac{\partial N_j}{\partial r} + \frac{N_j}{r} \frac{\partial N_i}{\partial r} - \frac{\partial N_i}{\partial z} \frac{\partial N_j}{\partial z} \right) \right] d\Omega \quad (6)$$

$$F_{1,i}^{ele} = \int_{ele} C_2 N_i d\Omega$$

$$F_{2,i}^{ele} = \int_{ele} C_4 N_i d\Omega \quad (7)$$

Appendix A reports the calculation of the element matrices above for the case of a three-node triangular element (linear shape functions).

Time discretization of Eqs. (3) and (4) can be obtained by the well-known Crank–Nicolson method (a central difference method) which has been proven to be unconditionally stable in the case of constant matrix coefficients [2].

Finally, the numerical formulation of the problems requires, at each gauss point of the finite element mesh, the numerical integration in time of the internal variable evolution laws (governing hydration degree, silica fume reaction degree, concentration of silicate polymers). As presented in the companion paper [1], these equations can be all expressed in the form $\dot{x} = f(x, h, T)$, where x represents an internal variable. A very effective method to integrate such a differential equation is to use the second order Runge–Kutta formula (midpoint method). By this approach x_{n+1} , i.e. the value of the internal variable at time t_{n+1} , can be estimated as

$$x_{n+1} \approx x_n + \Delta t_n f(x_{n+1/2}, h_{n+1/2}, T_{n+1/2}) \quad (8)$$

where x_n is the value of the internal variable at time t_n , Δt_n is the time increment, $x_{n+1/2} = (x_{n+1} + x_n)/2$, $h_{n+1/2} = (h_{n+1} + h_n)/2$, and $T_{n+1/2} = (T_{n+1} + T_n)/2$. At time $t_0 = 0$ (time of casting) all the internal variables are set to zero ($x_0 = 0$).

Remark 1. The discretized balance equations and the numerical evolution laws are both nonlinear and need to be solved by means of an iterative scheme. The numerical simulations performed in this study showed that an iterative scheme based on a global measure of convergence (e.g., norm of temperature and/or humidity vectors), provides satisfactory accuracy in the iterative solution of the internal variable evolution laws.

Remark 2. The system in Eqs. (3) and (4) do not include the boundary conditions. However, Dirichlet's boundary conditions can be directly imposed on the system of Eqs. (3) and (4) [3], whereas Cauchy's boundary conditions can be enforced approximately by considering an additional layer of material attached to the actual boundaries and imposing Dirichlet's boundary conditions on these fictitious boundaries. By changing the thickness of the additional layer, different heat and moisture surface emissivity coefficients can be simulated [3].

Remark 3. The discussed axis-symmetric numerical formulation can be also applied to the solution of two-dimensional problems. The only modification of the discretized equations consist in neglecting the term $(N_j \partial N_i / \partial r) / r$ appearing in the expressions of $K_{2,ij}^{ele}$ and $K_{4,ij}^{ele}$.

3. Calibration and validation procedure

The material properties needed to simulate, according to the present theory, moisture transport and heat transfer in high-per-

Table 1
Material properties with known or independently measurable value.

Material property name (unit)	Symbol	Typical value	Reference
Density (kg/m ³)	ρ	2400	[20]
Isobaric heat capacity (J/kg °C)	C_t	1100	[20]
Heat conductivity (W/m °C)	λ	2.3	[21]
Cement hydration enthalpy (kJ/kg)	\bar{Q}_c^∞	500	[22]
Silica fume reaction enthalpy (kJ/kg)	\bar{Q}_s^∞	780	[23]
Hydration activation energy/R (K)	E_{ac}/R	5000	[6]
Silica fume reaction activation energy/R (K)	E_{as}/R	9700	[14]
Diffusivity activation energy/R (K)	E_{ad}/R	2700	[3]
Silica fume efficiency (-)	SF^{eff}	0.9	[14,9]
Polymerization activation energy/R (K)	E_{ap}/R	6000	[24]
Hydration threshold for polymerization (-)	α_c^0	0.1	[1]
n/a (-)	k_c	0.253	[4]
n/a (-)	k_s	0.0	[1]
n/a (-)	k_{pc}	0.0	[1]

formance concrete can be subdivided into two categories. Material properties that have been already established in the past and that can be measured independently from the current theory (do not require a back analysis), belong to the first category. These properties are summarized in Table 1 along with typical values that can be used when specific experimental measurements are not available. These standard property values will be used throughout the rest of the paper unless otherwise specified. On the contrary, material properties whose calibration requires back analysis of the current theory, belong to the second category. These properties, referred hereinafter as free parameters of the model, are: hydration degree parameters, η_c , A_{c1} , and A_{c2} , SF reaction degree parameters, η_s , A_{s1} , and A_{s2} , sorption isotherm parameters, k_{vg}^c , k_{vg}^s , and g_1 , moisture diffusivity parameters, \bar{D}_0 , \bar{D}_1 , and n , polymer concentration parameter, A_{p1} , and chemically bound water parameter related to polymerization, k_{ps} .

The free parameters of the model can be calibrated on the basis of the following calibration procedure:

1. Considering a concrete mix without silica fume:

- Calibrate k_{vg}^c and g_1 by fitting experimental sorption/desorption isotherms relevant to two different values of hydration degree, which should remain constant during tests in order to decouple the calibration of the sorption isotherm from the calibration of the parameters related to cement hydration (step 1b). This can be only achieved in an approximate way because it is not possible to stop the hydration process while conducting the sorption/desorption tests. It is feasible, however, to obtain experimental sorption isotherms characterized by a small variation of the hydration degree (≤ 0.1) [5]. The calibration of k_{vg}^c and g_1 should be performed with reference to the mean value of the hydration degree during the test.
- Calibrate η_c , A_{c1} , and A_{c2} by fitting either temperature rise in an adiabatic calorimetric test [6] or the experimental hydration degree calculated as the ratio between the heat released in an calorimetric test and the total heat released at complete cement hydration [7].
- Calibrate \bar{D}_0 , \bar{D}_1 , and n by fitting experimental results of drying tests [3,8].

2. Considering the concrete mix in step 1 with the addition of silica-fume and keeping unaltered the already calibrated parameters:

- Calibrate k_{vg}^s by fitting sorption/desorption experimental data [5]. Same considerations made in step 1a apply here.
- Calibrate η_s , A_{s1} , and A_{s2} by fitting the difference in temperature rise (or heat development) for adiabatic calorimetric tests (or isothermal calorimetric tests) with and without (data used in step 1b) SF. Alternatively, η_s , A_{s1} , and A_{s2} can

- be calibrated by fitting direct measurement of the degree of pozzolanic reaction, which can be obtained by measuring the variation of CH content due to the presence of SF [9].
- (c) Calibrate A_{p1} by fitting experimental polymer concentration data that can be obtained by measuring the evolution of polymerized species in hydrated concrete mix [9].
- (d) Calibrate k_{ps} by fitting experimental data on chemically bound water in presence of polymerization (that is for sufficiently hydrated concrete) [10]. Considering that: (1) the chemically bound water is proportional to the polymers concentration through the parameter k_{ps} , (2) the polymers concentration is proportional to the parameter A_{p1} , and (3) polymerization only affects the formula of the chemically bound water, experimental data on chemically bound water can be actually used to calibrate directly the polymerization parameter $C_p = k_{ps}A_{p1}$. This allows eliminating step 2c for which experimental data is extremely rare and difficult to obtain.

It must be noted here that, in the current literature, a comprehensive study providing, for the same concrete, all experimental data needed for the calibration procedure outlined above, is not available. In most of the cases, experimental investigations tend to analyze specific aspects in relation to different mixes more than focusing on a thorough analysis of one single mix. In these cases, the only option left is an educated guess of the parameters that cannot be calibrated.

Once the calibration has been performed, the validation has to be carried out by simulating experimental data, relevant to the same concrete of the calibration, that has not been used in the cal-

ibration phase. In the validation phase, parameter adjustment is not permitted. In the following sections examples of calibration and validation will be presented and discussed.

4. Sorption/desorption isotherms

The calibration of the sorption isotherm parameters is discussed in this section. As discussed in the companion paper [1], the difference between sorption and desorption isotherms are neglected in this study as done in previous studies by other researchers [11]. This also permits to calibrate the sorption isotherm on the basis of desorption data, which are the most commonly available in the literature.

Desorption experimental data for two old concretes (2 years of age), labeled as BO and BH, were published in [12]. Both mixes were prepared with a type I Portland cement. The first mix (BO) was a standard concrete, characterized by $w/c = 0.48$ and $c = 300 \text{ Kg/m}^3$. On the contrary, the second mix (BH) was a high-performance concrete, characterized by $w/c = 0.26$, $c = 450 \text{ Kg/m}^3$, and containing silica fume ($s/c = 0.10$). With these material properties, one can obtain $\alpha_c^\infty = 0.73$ for mix BO, and $\alpha_c^\infty = 0.51$, $\alpha_s^\infty = 0.87$ for mix BH [1]. These values can be assumed to be the hydration degree and the degree of SF reaction at the time of the tests. With this assumption, the best fitting of the experimental data without SF (Fig. 1a) can be obtained by setting $k_{vg}^c = 0.2$ and $g_1 = 1.5$. The best fitting of the experimental data with silica fume (Fig. 1b) can be obtained by adopting the previously identified parameters ($k_{vg}^c = 0.2$, $g_1 = 1.5$) and by setting $k_{vg}^s = 0.36$.

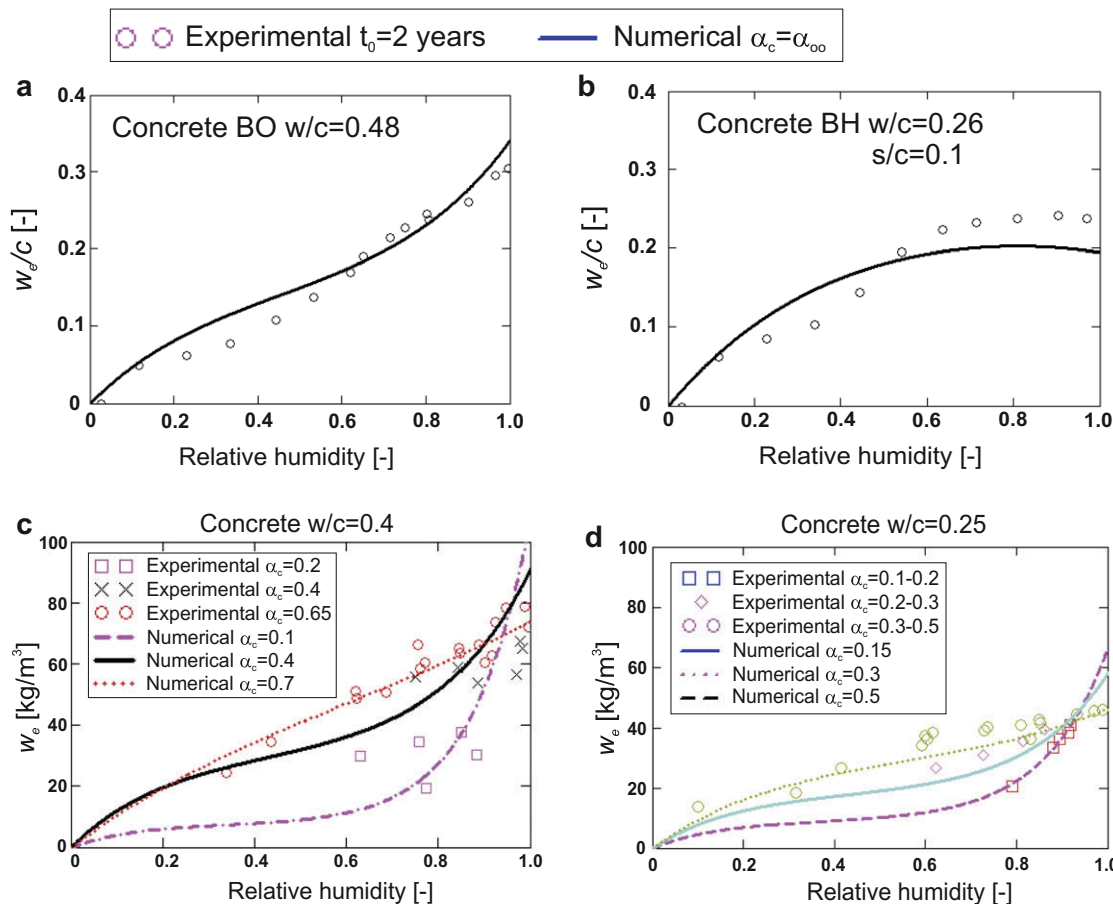


Fig. 1. Fitting of experimental desorption isotherms for concrete mixes with various water-to-cement ratios and various degrees of hydration.

In Ref. [5] experimental desorption data, relevant to two different concrete mixes characterized by two water-to-cement ratios, were reported. The first mix ($w/c = 0.4$) was tested at three different ages characterized by α_c varying from 0.1, 0.3, and 0.5 to 0.3, 0.5, and 0.6, respectively. The numerical simulations were performed by assuming an average hydration degree, $\alpha_c = 0.15, 0.4$, and 0.65, respectively, for the three cases. Fig. 1c shows the best fitting of the experimental data obtained by setting, again, $k_{vg}^c = 0.2$ and $g_1 = 1.5$. As shown in Fig. 1d, the same parameters can be also used to fit the desorption data of the second mix ($w/c = 0.25$) tested at four different ages. For this case, the experimental hydration degree ranges and the mean values adopted in the numerical calculations are reported in the figure legend.

For all the experimental data sets analyzed in this section, the agreement between the theory and the experiments can be considered good even though, for some of the tests, the scatter of the experimental data is relatively high.

5. Isothermal calorimetric tests

For ordinary portland cement, the evolution of the hydration degree can be obtained from the evolution of chemically bound water, whose measurement can be, in turn, utilized to calibrate the hydration degree parameters. The experimental data obtained by Pane and Hansen [13], who measured the evolution in time of the chemically bound water in sealed samples of cement paste cured isothermally at three different temperatures (9, 23, and 34 °C), is analyzed in this section.

The tested cement paste was characterized by $c = 438 \text{ Kg/m}^3$, $w/c = 0.4$, and $\alpha_c^\infty = 0.72$. In addition, a latent heat of hydration equal to $\tilde{Q}_c^\infty = 439.0 \text{ kJ/kg}$ was reported by the authors of the experimental investigation [13].

Since, in these tests, the temperature and humidity fields do not feature significant spatial gradients, the numerical simulations were carried out on a single element mesh subjected to boundary conditions corresponding to isothermal heat exchange and without water mass exchange.

The best fitting of the experimental data points relevant to $T = 9 \text{ }^\circ\text{C}$ was obtained by the parameters reported on the second column of Table 2. It must be noted that, since desorption data was not available, the sorption isotherm parameters discussed in the previous section were adopted. Finally, the simulations re-

lent to the other temperatures were performed without changing the parameters for validation purposes.

Fig. 2 shows the comparison between the experiments and the numerical simulations with reference to the chemically bound water normalized by its asymptotic value. The agreement is excellent and the theory correctly predict faster hydration for higher temperatures. As discussed in [1], this effect is captured automatically through the Arrhenius-type dependence of the hydration process on temperature. Fig. 2 also shows that the final value of the chemically bound water (and, similarly, the degree of hydration) does not depend on temperature.

6. Adiabatic calorimetric tests

The experimental investigation of Bentz et al. [14] on conventional and high-performance concretes aimed at the characterization of their adiabatic heat signature is considered herein. Bentz et al. [14] measured the temperature increase under adiabatic conditions for a large variety of concrete mixes with and without SF. In Table 3, the first four columns report density, cement content, water-to-cement ratio, and silica-to-cement ratio, respectively, for 16 of these mixes. The fifth and the seventh columns of the same Table report the asymptotic hydration degree and the asymptotic silica fume reaction degree, calculated on the basis of Eqs. 19, 20, 24 and 26 in [1]. These values are in very good agreement with the values of the same quantities calculated, with reference to a concrete age of 3 years, by Bentz et al. [14] through a three-dimensional microstructural model (sixth and eighth columns of Table 3).

The values $Q_c^\infty = 520 \text{ kJ/kg}$, $E_{ac}/R = 5490 \text{ K}$, $E_{as}/R = 9620 \text{ K}$ can be assumed for all 16 mixes based on data reported in [14]. It is worth noting that the assumed value for Q_c^∞ is very good agreement with (only 7% higher than) the value calculated from the enthalpy of complete hydration of the major phases of cement [14].

Similarly to the previous section, the numerical simulations of these experiments were performed by a single element mesh. Boundary conditions not allowing mass and heat exchange through the external surfaces were imposed to simulate an adiabatic system.

In the absence of specific measurements, the sorption isotherm parameters were assumed to be equal to the ones optimized in Section 4. The hydration degree parameters were calibrated by the best fitting of the adiabatic temperature rise for Mix 1, which does not include SF. Then, the adiabatic temperature rise for Mix 13, which includes SF, was used to calibrate the SF reaction degree parameters. The optimized parameters are reported in the third column of Table 2. The numerical simulations of the other 14 mixes were performed for validation.

Figs. 3–6 show comparison between the experimental data and the numerical simulations. Symbols are the experimental data points, lines represent the results obtained by the present model with (solid line) and without (dashed line) the effect of the SF reaction degree. As one can see, without modeling the SF reaction, temperature rise is underestimated by up to 10%. On the contrary, with the use of the full theory, the agreement is excellent for all 16 mixes. These results clearly show the proposed model can be reliably employed to predict the temperature rise and the heat production of a wide variety of concrete mixes with and without SF.

7. Self-desiccation tests

The third numerical example deals with self-desiccation, that is the reduction of relative humidity in early age sealed samples due to water consumption associated with cement hydration.

The material properties and boundary conditions (sealed conditions for mass exchange at constant temperature) correspond to those in the experimental study of Lura et al. [15], who measured

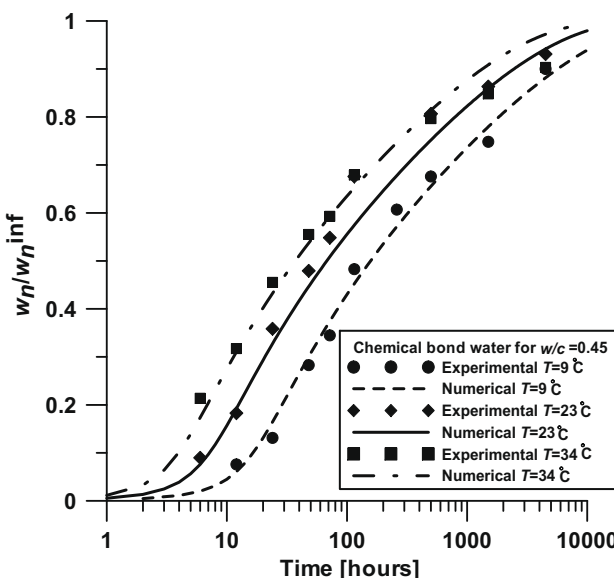


Fig. 2. Numerical simulations of the experimental data of Pane and Hansen [13]: evolution of the chemically bound water under different isothermal conditions.

Table 2

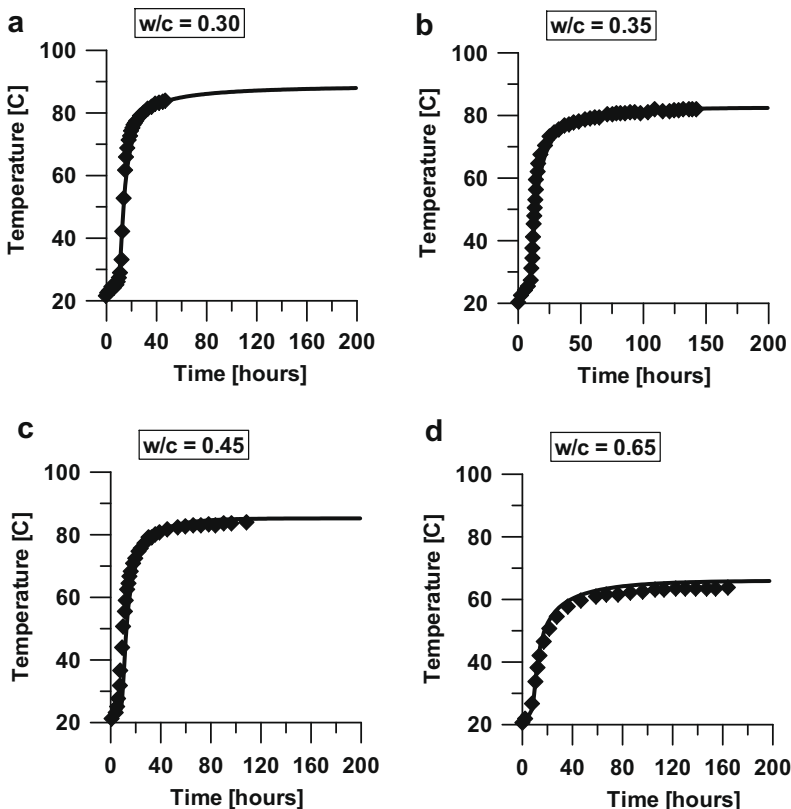
Values of the free parameters used in the numerical simulations.

Par. (unit)	Section 5	Section 6	Section 7	Section 8	Section 9	Section 10
$g_1 (-)$	1.5	1.5	1.75	1.2	1.7	1.55
$k_{eg}^c (-)$	0.2	0.2	0.2	0.255	0.11	0.18
$K_{eg}^c (-)$	–	0.36	0.36	–	–	–
$A_{c1} (\text{h}^{-1})$	1.41×10^7	20×10^7	10×10^7	1.5×10^7	4×10^7	3.5×10^7
$A_{c2} (-)$	5×10^{-3}	1×10^{-6}	1×10^{-6}	5×10^{-2}	5×10^{-2}	5×10^{-3}
$\eta_c (-)$	8	6.5	5.5	8	8.5	8
$A_{s1} (\text{h}^{-1})$	–	5×10^7	6×10^7	–	–	6×10^7
$A_{s2} (-)$	–	1×10^{-6}	1×10^{-6}	–	–	1×10^{-6}
$\eta_s (-)$	–	9.5	9.5	–	–	9
$C_p (\text{h}^{-1})$	–	–	0.875×10^4	–	–	0.875×10^4
$\bar{D}_0 (\text{m}^2/\text{h})$	–	–	–	0.085	0.0024	0.009
$\bar{D}_1 (\text{m}^2/\text{h})$	–	–	–	6	3.22	8
$n (-)$	–	–	–	3	3.25	4.5

Table 3

Density, cement content, water-to-cement ratio, silica-to-cement ratio, ultimate degree of hydration, and ultimate degree of silica fume reaction for concrete mixes studied by Bentz et al. [14].

	$\rho (\text{kg/m}^3)$	$c (\text{kg/m}^3)$	w/c	s/c	α_c^∞	α_c (3 years) Ref. [14]	α_s^∞	α_s (3 years) Ref. [14]
1	2443	529.5	0.30	0.0	0.63	0.66	–	–
2	2439	455.3	0.35	0.0	0.66	0.74	–	–
3	2367	438.1	0.45	0.0	0.72	0.87	–	–
4	2366	274.7	0.65	0.0	0.80	0.87	–	–
5	2447	474.8	0.30	0.05	0.60	0.62	0.87	0.66
6	2430	483.9	0.30	0.10	0.57	0.57	0.87	0.59
7	2318	453.2	0.30	0.30	0.56	0.48	0.40	0.37
8	2488	453.0	0.35	0.20	0.59	0.59	0.70	0.53
9	2354	455.3	0.45	0.05	0.70	0.80	0.87	0.88
10	2421	344.1	0.45	0.10	0.68	0.77	0.87	0.77
11	2413	323.3	0.45	0.20	0.65	0.72	0.78	0.63
12	2406	333.8	0.45	0.30	0.65	0.68	0.53	0.50
13	2381	307.2	0.55	0.20	0.70	0.78	0.79	0.74
14	2358	281.9	0.65	0.05	0.78	0.88	0.87	0.94
15	2340	300.2	0.65	0.10	0.76	0.85	0.87	0.92
16	2347	295.1	0.65	0.30	0.74	0.81	0.53	0.64

**Fig. 3.** Experimental investigation of Bentz et al. [14]: experimental (data points) and numerical (solid lines) adiabatic temperature rise curves for concrete with different values of water-to-cement ratio and without silica fume.

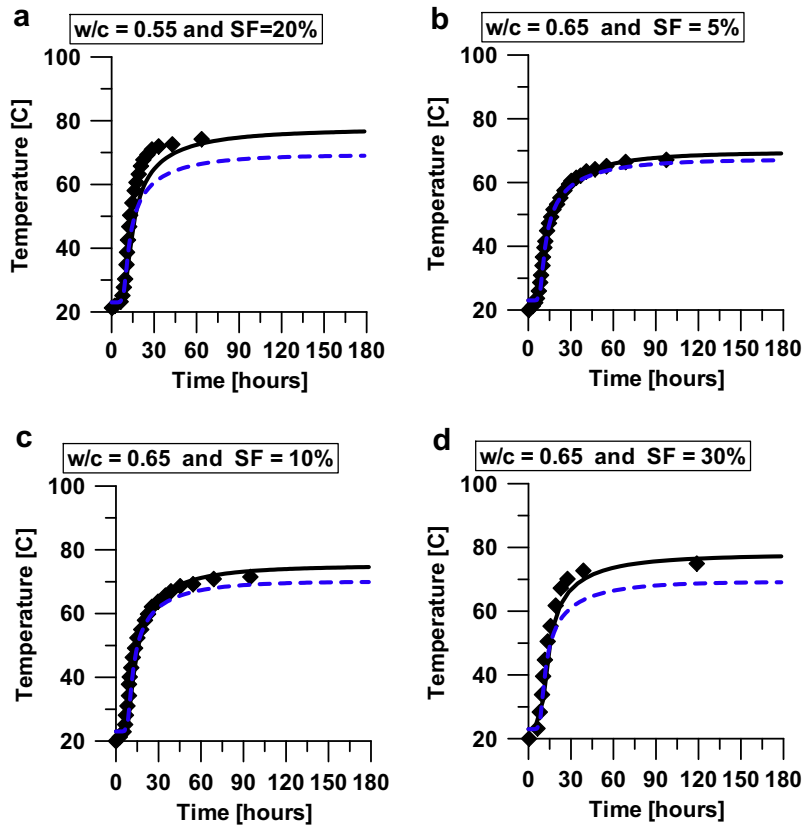


Fig. 4. Experimental investigation of Bentz et al. [14]: experimental (data points) and numerical (solid and dashed lines) adiabatic temperature rise curves for concrete with high values of water-to-cement ratio and silica fume. Dashed lines represent model results obtained neglecting the SF reaction.

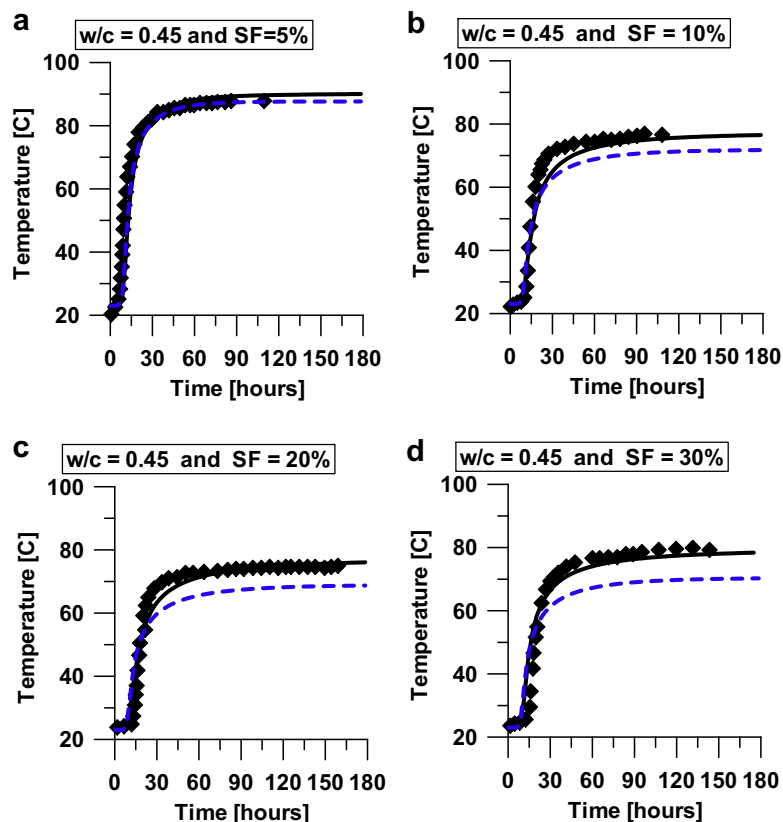


Fig. 5. Experimental investigation of Bentz et al. [14]: experimental (data points) and numerical (solid and dashed lines) adiabatic temperature rise curves for concrete with medium values of water-to-cement ratio and silica fume. Dashed lines represent model results obtained neglecting the SF reaction.

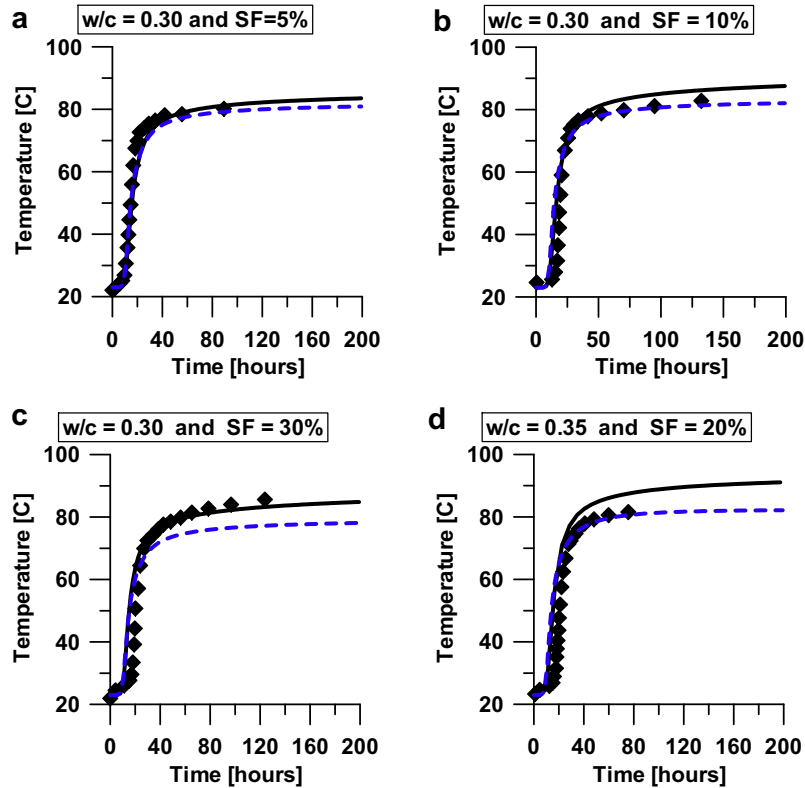


Fig. 6. Experimental investigation of Bentz et al. [14]: experimental (data points) and numerical (solid and dashed lines) adiabatic temperature rise curves for concrete with low values of water-to-cement ratio and silica fume. Dashed lines represent model results obtained neglecting the SF reaction.

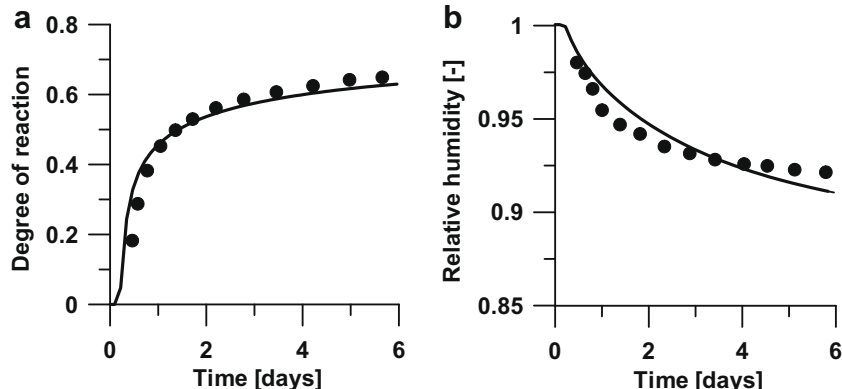


Fig. 7. Numerical simulations of the experimental data of Lura et al. [15] on high-performance cement paste: evolution in time of (a) degree of reaction and (b) relative humidity.

the development of the overall degree of reaction and relative humidity during the initial 6 days after casting in a cement paste characterized by $w/c = 0.37$, and $s/c = 0.052$. According to these material properties, one has $\alpha_c^\infty = 0.653$ and $\alpha_s^\infty = 0.9$.

The overall degree of reaction, referred hereinafter as α_r , is defined as the ratio between the heat measured in the isothermal calorimetric test, Q_r , and the heat developed at the completion of all chemical reactions, Q_r^∞ . One can write

$$\alpha_r(t) = \frac{Q_r(t)}{Q_r^\infty} = \frac{\alpha_c(t)c\tilde{Q}_c^\infty + \alpha_s(t)s\tilde{Q}_s^\infty}{\alpha_c^\infty c\tilde{Q}_c^\infty + \alpha_s^\infty s\tilde{Q}_s^\infty} \quad (9)$$

Again, since temperature and humidity fields with negligible gradient characterize these tests, a single element mesh was employed in the numerical simulations. The best fitting of reaction degree and relativity humidity evolution in time was obtained by the

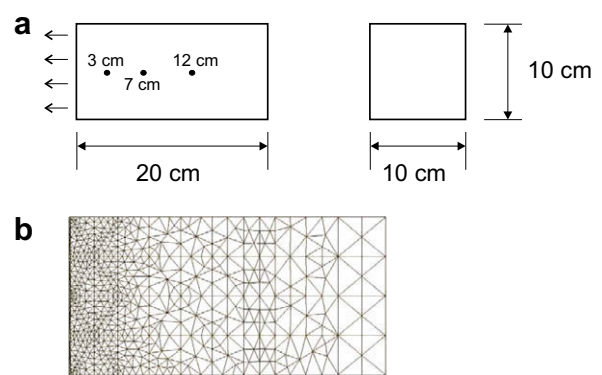


Fig. 8. Numerical simulations of the experimental data of Kim and Lee [17]: (a) geometry and (b) finite element mesh.

parameters reported in the fourth column of Table 2. Fig. 7a and b show the comparison between the experimental data and numerical results and the agreement is very good. In this case, no data was available for validation.

8. Drying tests

In the previous sections, calibration and validation have focused on experimental data featuring temperature and humidity fields without (or negligible) spatial gradients. Consequently, the numerical results were independent of the moisture permeability, whose effect is analyzed herein with reference to the experimental investigations of Kim and Lee [17] on moisture drying at early ages.

Drying occurs when concrete is exposed to ambient air with a relative humidity smaller than the relative humidity of the specimen. The imbalance of the relative humidity at the boundaries causes an outward flow of water, which, in turn, leads to moisture diffusion from the core towards the external surfaces of the specimens and to nonuniform relative humidity distributions. In addition, at the early ages, the entire process is influenced by the self-desiccation phenomenon.

Kim and Lee [17] measured the nonuniform moisture distributions in concrete samples, relevant to three different concrete mixes, exposed to ambient air with 50% relative humidity. The three mixes were characterized by cement content, water-to-cement ratio, and density equal to 541, 423, 310 Kg/m³, 0.28, 0.4, 0.68, and 2394, 2344, 2257 Kg/m³, respectively. Additional information on the chemical characteristics of the mix compounds and concrete compositions can be found in [17]. The tested specimens were prisms (10 × 10 × 20 cm), which were moist-cured before drying. Two different ages were considered: $t_0 = 3$ and 28 days. The internal relative humidity was measured at the distance of 3, 7, and 12 cm from the exposed surface (Fig. 8a), which was one of the 10 × 10 cm square bases. The other five sides were sealed to generate a uniaxial moisture diffusion. In addition, completely sealed cubic specimens were also used to measure the variation of relative humidity due to self-desiccation only.

The numerical simulations of these tests were performed by using the plane finite element mesh showed in Fig. 8b. On the exposed surface, Cauchy's boundary conditions were imposed by an equivalent surface thickness of 0.75 mm (see Section 2).

For the three mixes, the asymptotic degree of hydration can be calculated as 0.61, 0.694, and 0.8, respectively. Since sorption iso-

therm data and hydration degree data were not available for these concretes, the sorption isotherm parameters and hydration degree parameters were calibrated all together by simulating the self-desiccation experiments relevant to $w/c = 0.4$ and age of 3 and 28 days (solid curves in Fig. 9a and b). The permeability parameters were calibrated by simulating drying experimental data relevant to $w/c = 0.4$ and age of 3 days (Fig. 10b). The optimized parameters are reported in the fifth column of Table 2. The numerical simulations of the other available data served as validation of the model.

Figs. 9–11 show the comparison between the numerical results as the experimental data for all the simulations. The agreement is overall excellent, proving that the present model can be used reliably to estimate moisture diffusion in normal and high-performance concretes.

Fig. 9a and b show, for the various concretes, the evolution in time of relative humidity for the sealed specimens subjected to self-desiccation after moist-curing for 3 and 28 days, respectively. The model correctly predicts higher relative humidity decrease for low water-to-cement ratios at early ages. The initial relative humidity after moist-curing is slightly less than one for low water-to-cement ratios suggesting that the water provided through the moist-curing was not enough to maintain complete saturation of these concretes.

Fig. 10a, b, and c show, for the three considered water-to-cement ratios, the evolution in time of relative humidity at the three different locations mentioned previously, after 3 days of moist-curing. When drying begins, similarly to the previous case, the initial internal relative humidity in specimens with low water-to-cement ratio is less than the one in specimens with high water-to-cement ratio. In addition, data characterized by high water-to-cement ratio shows full saturation at the beginning of drying.

Furthermore, the model simulates correctly the spatial gradient of relative humidity, which decreases with the distance from the exposed surface. By comparing self-desiccation and drying data, both the numerical simulations and the experimental data suggest that, in the inner regions of the specimens, the variation of relative humidity is mainly due to self-desiccation in the case of low water-to-cement ratios (slower moisture diffusion and higher self-desiccation) and to drying in the case of high water-to-cement ratios (faster moisture diffusion and lower self-desiccation). This is in agreement to the fact that, typically, concretes with low water-to-cement ratio feature a denser microstructure

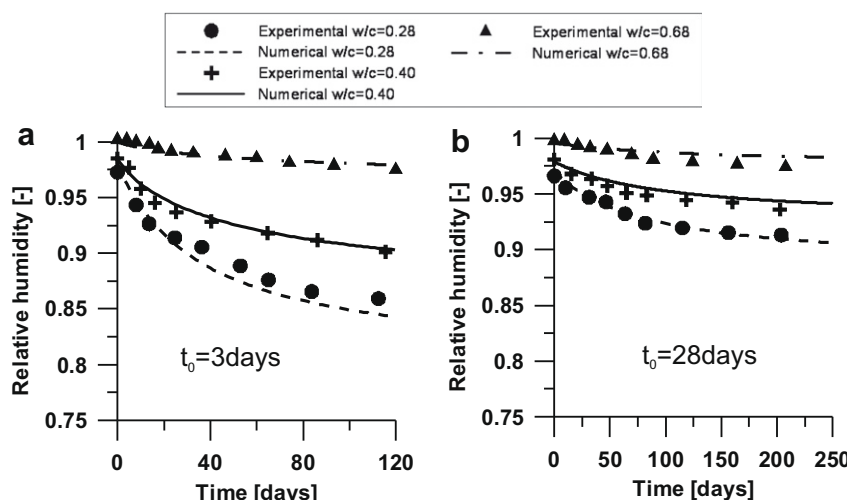


Fig. 9. Numerical simulations of the experimental data of Kim and Lee [17]: relative humidity vs. time due to self-desiccation for (a) $t_0 = 3$ day and (b) $t_0 = 28$ day.

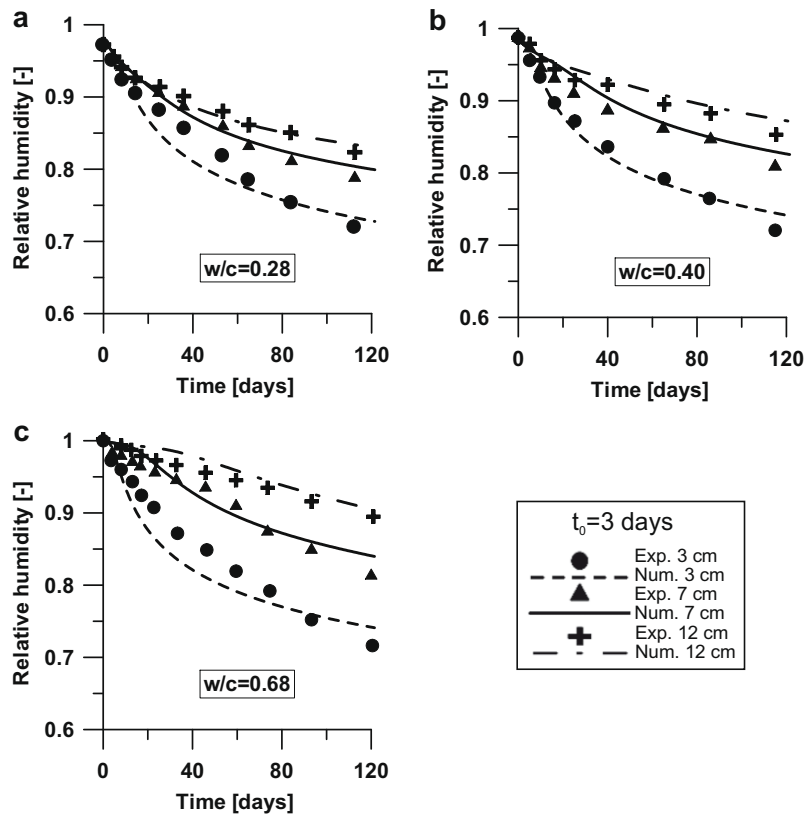


Fig. 10. Numerical simulations of the experimental data of Kim and Lee [17]: relative humidity vs. time with $t_0 = 3$ day due to moisture diffusion and self-desiccation for concrete with different water-to-cement ratios and at different positions in the specimen.

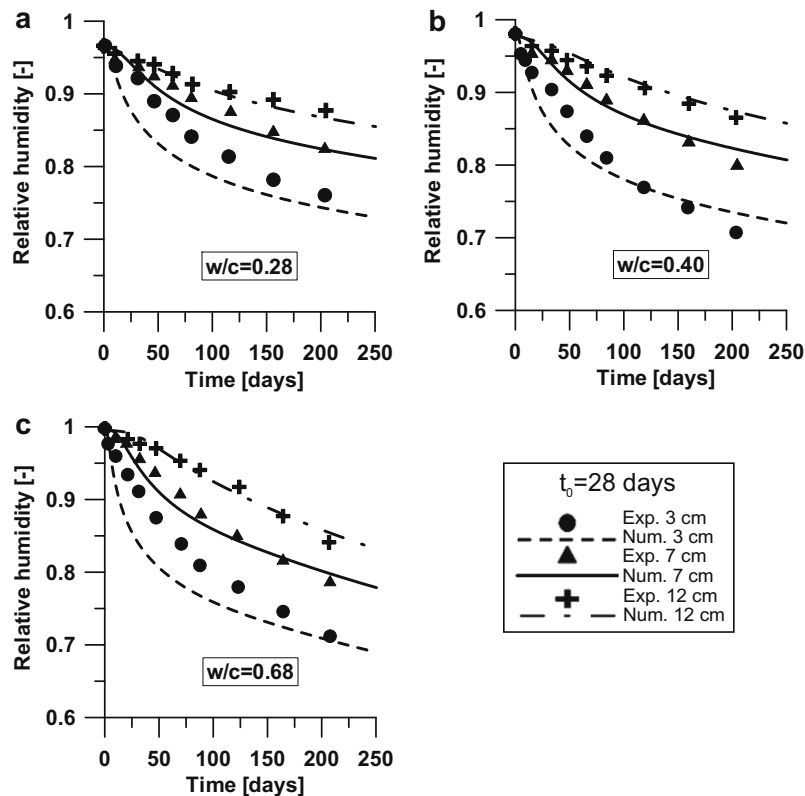


Fig. 11. Numerical simulations of the experimental data of Kim and Lee [17]: relative humidity vs. time with $t_0 = 28$ day due to moisture diffusion and self-desiccation for concrete with different water-to-cement ratios at different positions in the specimen.

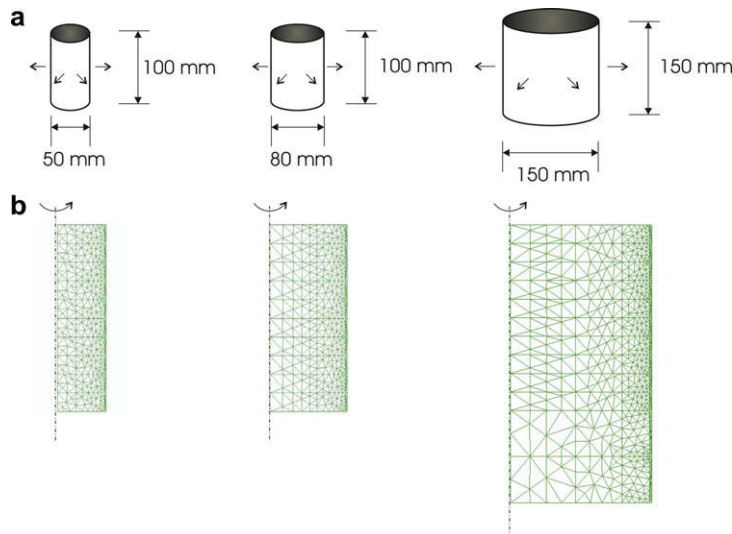


Fig. 12. Numerical simulations of the experimental data of Ayano and Wittmann [16]: (a) geometry and (b) finite element mesh.

and are characterized by higher consumption of water during hydration.

Similar observations can be made with reference to Fig. 11a, b, and c relevant to drying data at the age of 28 days.

9. Size-effect on moisture loss

The proposed model is also able to predict the size-effect on moisture loss, that is the reduction of the overall moisture content as function of specimen size. The moisture loss (by weight) can be calculated by subtracting from the initial water content, w_0 , the sum of non-evaporable water, w_n and evaporable water, w_e . By integrating this difference over the volume, V , of the specimen one can obtain the average moisture loss, W_{loss} , as

$$W_{loss} = w_0 V - \int_V (w_n + w_e) dV \quad (10)$$

In the experimental investigation of Ayano and Wittmann [16], the average moisture loss was measured for three cylindrical concrete specimens characterized by different diameters, $\phi = 50$, 80, and 150 mm, and lengths, $L = 100$, 100, and 150 mm, respectively (Fig. 12a). The moisture loss was due to exposure to ambient air

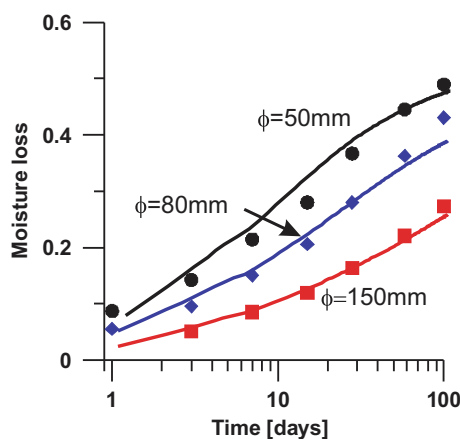


Fig. 13. Numerical simulations of the experimental data of Ayano and Wittmann [16] on moisture loss: symbols are experimental data points and solid lines are numerical results.

with relative humidity of 45%. The top and the bottom surfaces of the cylinders were sealed in order to generate a radial water diffusion. The tested concrete was characterized by $c = 400 \text{ kg/m}^3$, $\rho = 2334 \text{ Kg/m}^3$, $\bar{Q}_c^\infty = 400 \text{ KJ/kg}$, and $w/c = 0.5$. For this value of water-to-cement ratio one has $\alpha_c^\infty = 0.74$.

The three specimens were modeled through axis-symmetric finite element meshes, which are shown in Fig. 12b. The parameters of the model were calibrated by simulating the specimen with $\phi = 100 \text{ cm}$ and their optimized values are reported in the sixth column of Table 2. The simulation of the other specimens served as validation. Fig. 13 shows the comparison between the experimental and the numerical results in terms of average water loss normalized with respect to the initial total water content $W_0 = w_0 V$. The agreement between experiments and simulations is excellent and the model is able to predict with great accuracy the size-effect in moisture loss.

10. Effect of curing conditions on moisture content

In this section the numerical simulations of the experimental results obtained by Persson [10,18,19] are presented. In this experimental investigation, chemically bound (non-evaporable) water and internal relative humidity were measured in concrete specimens subjected to air, water, and sealed curing, over a period of 450 days. Eight different concrete mixes, characterized by various values of water-to-cement ratio and cement content, were studied. Four mixes also included silica fume. The compositions of these mixes are reported in Table 4 where one can also see the calculated ultimate degree of hydration and ultimate degree of silica reaction.

Table 4

Cement content, water-to-cement ratio, silica-to-cement ratio, ultimate degree of hydration, and ultimate degree of silica fume reaction for concrete mixes studied by Persson [10,18,19].

	$\rho (\text{kg/m}^3)$	$c (\text{kg/m}^3)$	w/c	s/c	α_c^∞	α_s^∞
1	2513	456	0.25	0.0	0.582	–
2	2469	400	0.33	0.0	0.646	–
3	2441	303	0.46	0.0	0.727	–
4	2424	299	0.58	0.0	0.772	–
5	2533	484	0.22	0.1	0.495	0.792
6	2500	476	0.24	0.1	0.515	0.864
7	2456	389	0.36	0.1	0.67	0.9
8	2451	298	0.48	0.1	0.734	0.9

The chemical characteristic of cement, aggregate, silica fume, and additives can be found in [10]. The tested specimens were circular slabs of 1 m diameter and 0.1 m thickness. For air and water curing, the flat sides of the slabs were covered by thick layers of epoxy resin to impose only radial moisture transport. For sealed curing, also the external circular surface was treated with epoxy resin in order to obtain perfectly sealed conditions. Temperature and humidity of the ambient air were recorded during the air curing tests and their evolution in time (Fig. 14a and b) provides the essential boundary conditions for the numerical simulation of these tests. For both air and water curing, relative humidity measurements were obtained through cast-in plastic probes placed at 50, 150 and 350 mm from the exposed surface [10].

The model parameters were calibrated by fitting the experimental results relevant to Mix 2 (without silica fume) and Mix 7 (with silica fume), both featuring a water-to-cement ratio close to the average water-to-cement ratio (0.365) of the eight mixes. In particular, the optimized parameters, reported in the seventh

column of Table 2, were obtained by the best fitting of self-desiccation data (Figs. 16b and 21b), chemically bound water data (Figs. 16e and 21d), and drying data (Figs. 16d and 21e). The same model parameters were used to simulate the behavior of the other six mixes for validation purpose. Comparison between the experimental data and the numerical predictions are shown in Figs. 15–22. Each figure is relevant to a different concrete Mix and overall the agreement is good for all eight mixes.

Sub-figures a, c, and e in Figs. 19–22 show the chemically bound water (w_n) normalized with respect to cement content (c), for sealed conditions, air curing, and water curing, respectively. Both the experimental data and the numerical results show that the chemically bound water varies slightly under different curing conditions while it increases for increasing water-to-cement ratio. At the end of the tests (450 days), w_n/c shows more than 30% increase (from about 0.15 to about 0.2) as w/c increases from 0.25 to 0.58 (Figs. 15a and 18a). The presence of SF reduces the amount of chemically bound water but, at the same time,

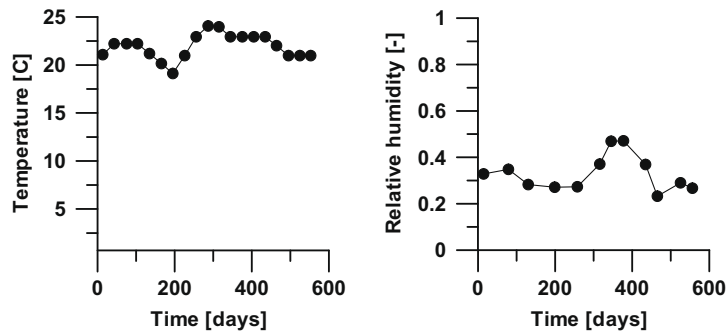


Fig. 14. Data by Persson [10,18,19]: measured air temperature and relative humidity during air curing.

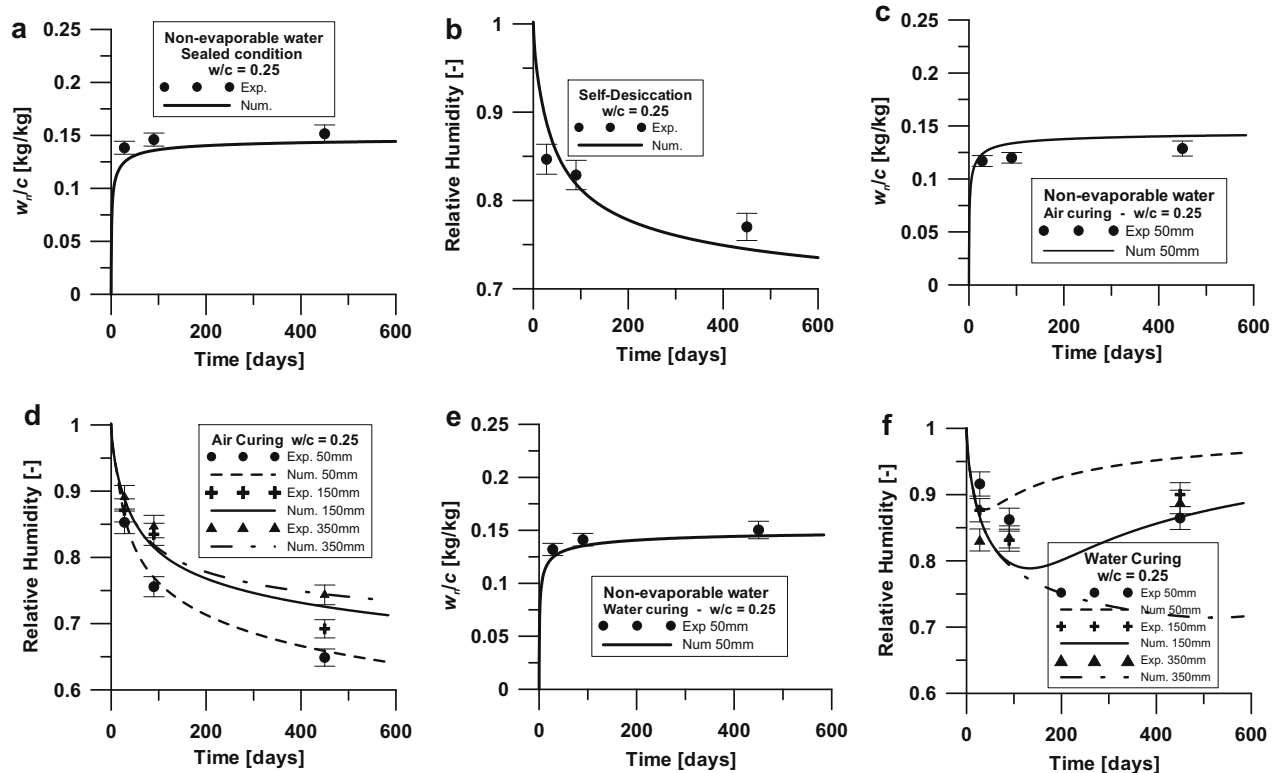


Fig. 15. Data by Persson [10,18,19], concrete Mix 1: non-evaporable water and relative humidity under sealed conditions (a, b), air curing (c, d), and water curing (e, f).

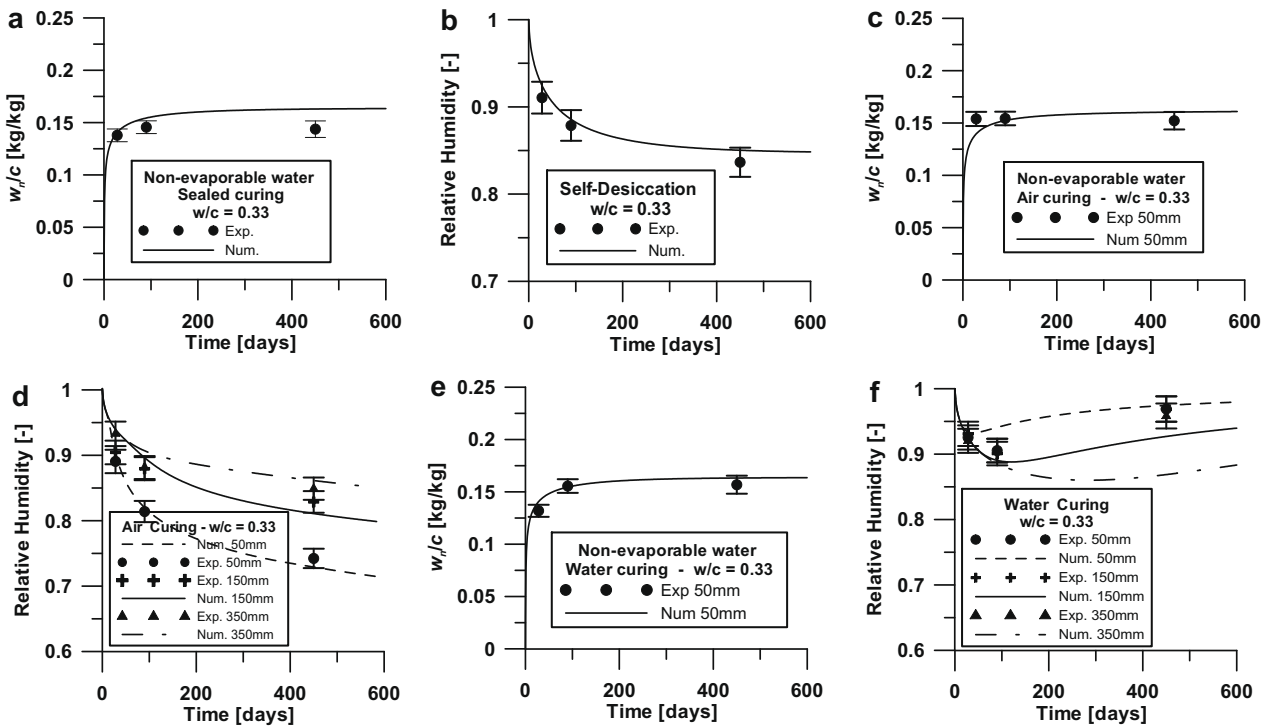


Fig. 16. Data by Persson [10,18,19], concrete Mix 2: non-evaporable water and relative humidity under sealed conditions (a, b), air curing (c, d), and water curing (e, f).

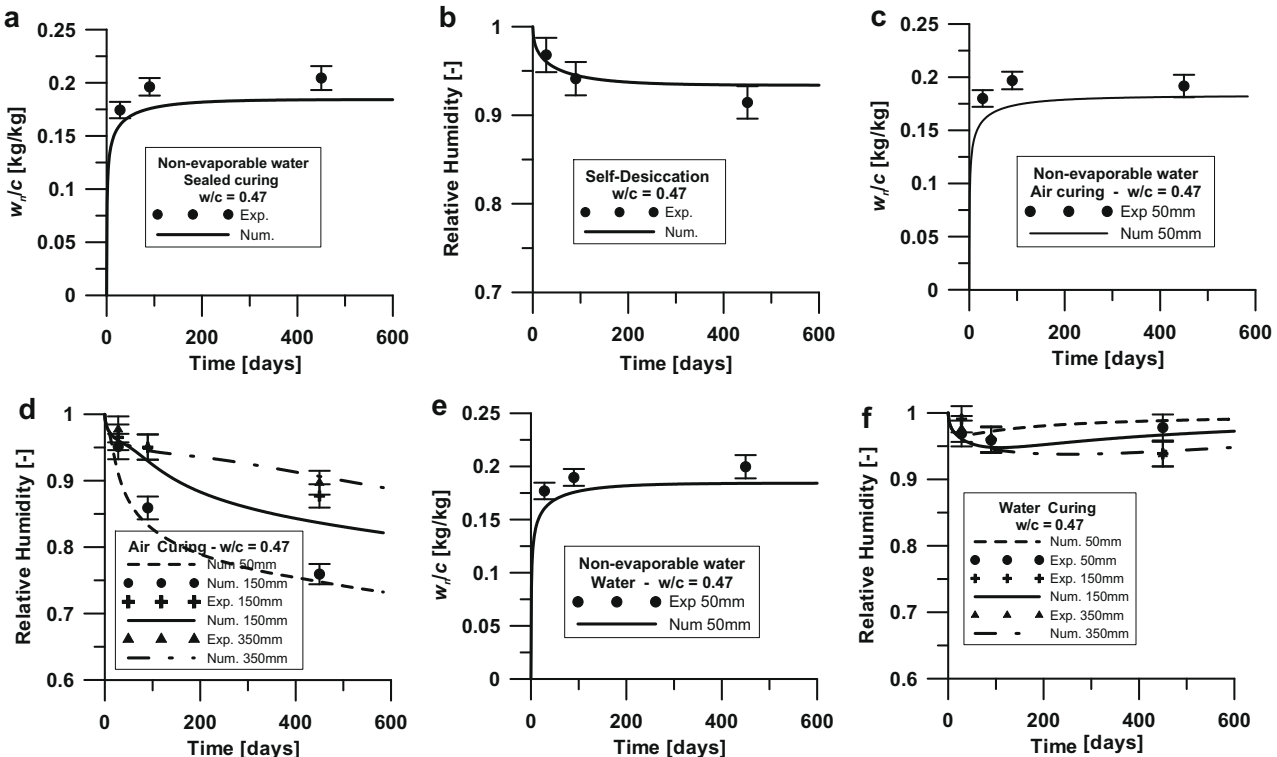


Fig. 17. Data by Persson [10,18,19], concrete Mix 3: non-evaporable water and relative humidity under sealed conditions (a, b), air curing (c, d), and water curing (e, f).

emphasizes its increase for increasing water-to-cement ratio. At the end of the tests (450 days), mixes with $s/c = 0.1$ show a 70% increase of w_n/c from about 0.1 for $w/c = 0.22$ (Fig. 19a) to about 0.17 for $w/c = 0.48$ (Fig. 22a). In addition, for these mixes,

the chemically bound water does not monotonically increase with time toward an asymptotic value, but rather shows a tendency to decrease after about 100 days of curing. This is due to silicate polymerization, which produces free evaporable water. For com-

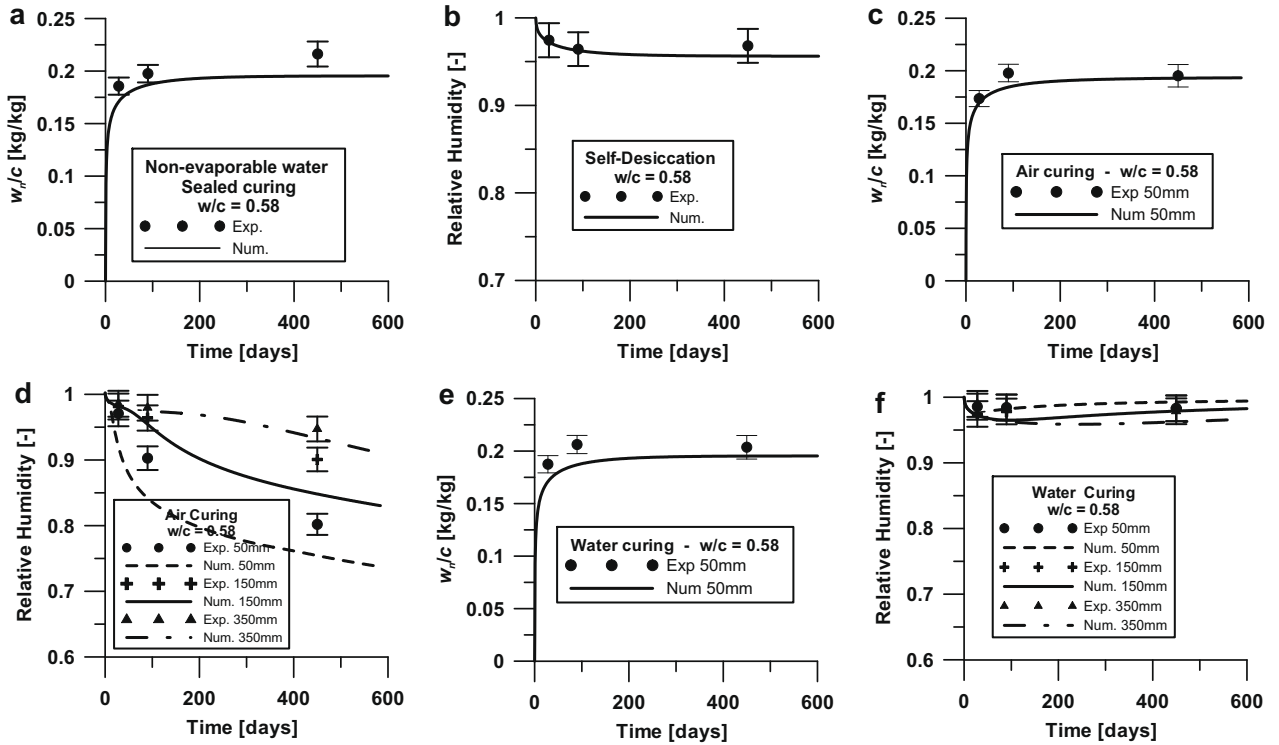


Fig. 18. Data by Persson [10,18,19], concrete Mix 4: non-evaporable water and relative humidity under sealed conditions (a, b), air curing (c, d), and water curing (e, f).

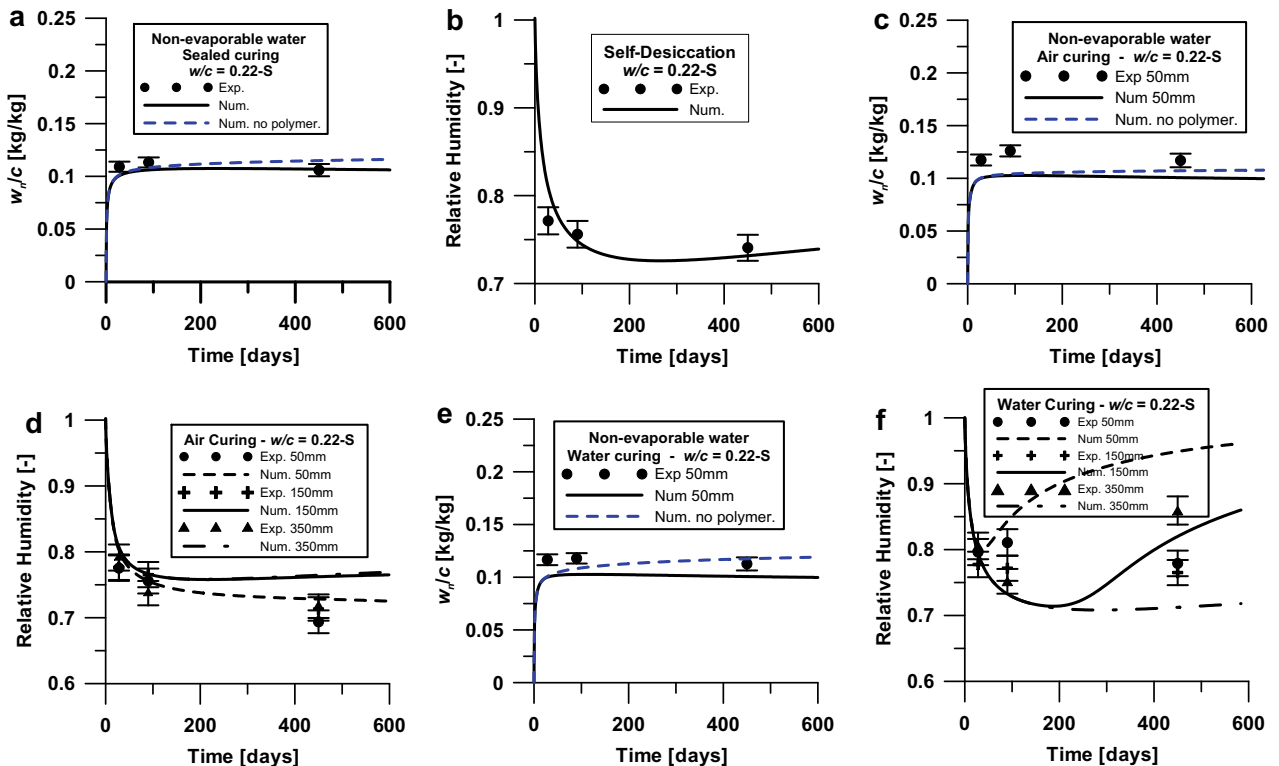


Fig. 19. Data by Persson [10,18,19], concrete Mix 5: non-evaporable water and relative humidity under sealed conditions (a, b), air curing (c, d), and water curing (e, f).

completeness, sub-figures a, c, and e in Figs. 19–22 show both the numerical results with (solid line) and without (dashed line) the effect of the polymerization.

Sub-figures b in Figs. 19–22 show the evolution of relative humidity under sealed conditions (self-desiccation). The relative humidity decreases with time and its reduction is higher

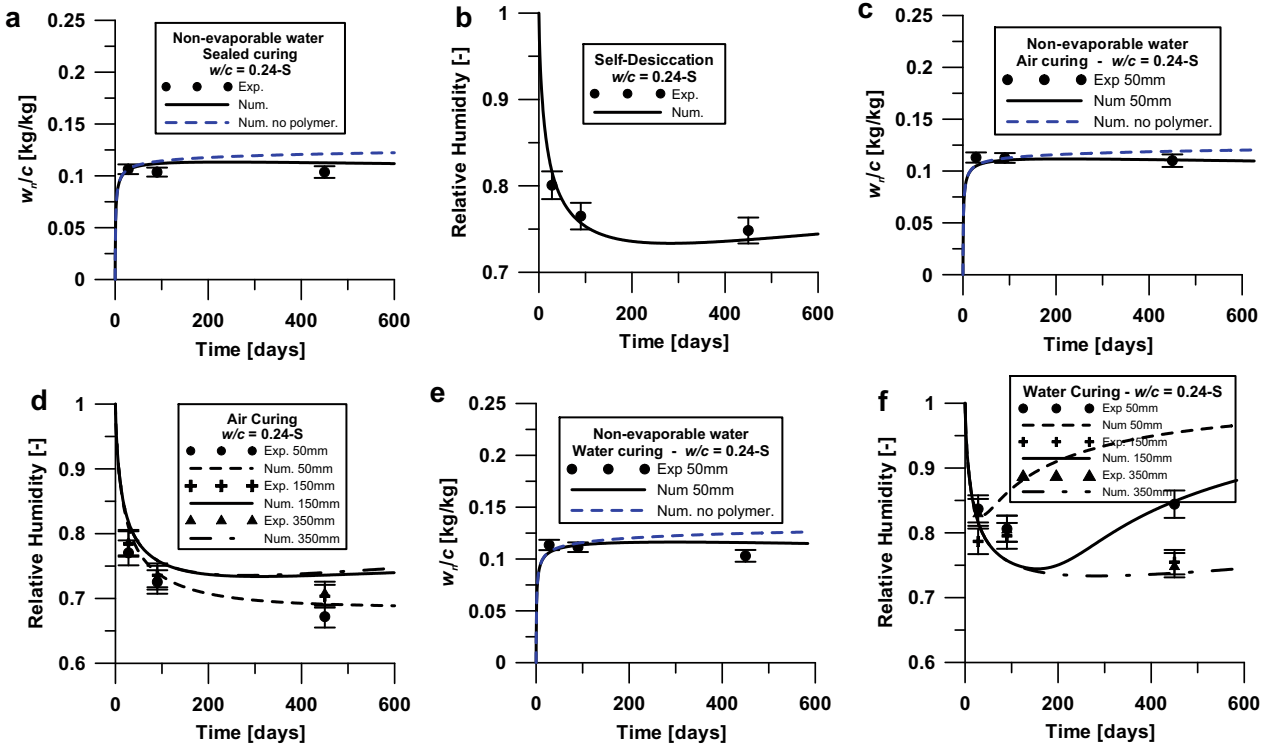


Fig. 20. Data by Persson [10,18,19], concrete Mix 6: non-evaporable water and relative humidity under sealed conditions (a, b), air curing (c, d), and water curing (e, f).

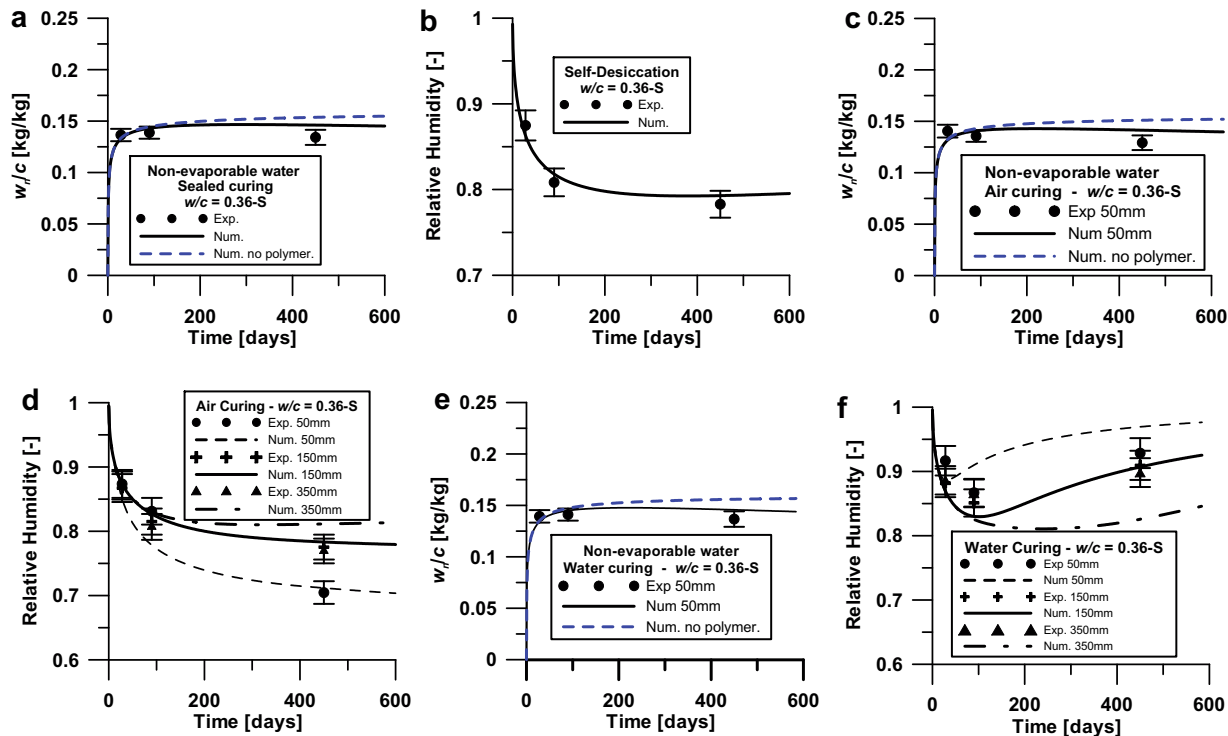


Fig. 21. Data by Persson [10,18,19], concrete Mix 7: non-evaporable water and relative humidity under sealed conditions (a, b), air curing (c, d), and water curing (e, f).

for lower water-to-cement ratio: at 450 days $h \approx 0.75$ (−25%) for $w/c = 0.25$ and $h \approx 0.95$ (−5 %) for $w/c = 0.58$. The presence of silica fume further intensifies the self-desiccation process. With $s/c = 0.1$, the relative humidity drops to 0.75 (−25%) for $w/c =$

0.22 and to less than 0.9 (−10%) for $w/c = 0.48$, after only 100 days of curing.

Sub-figures d in Figs. 19–22 show the evolution of relative humidity at three different locations in specimens subjected to

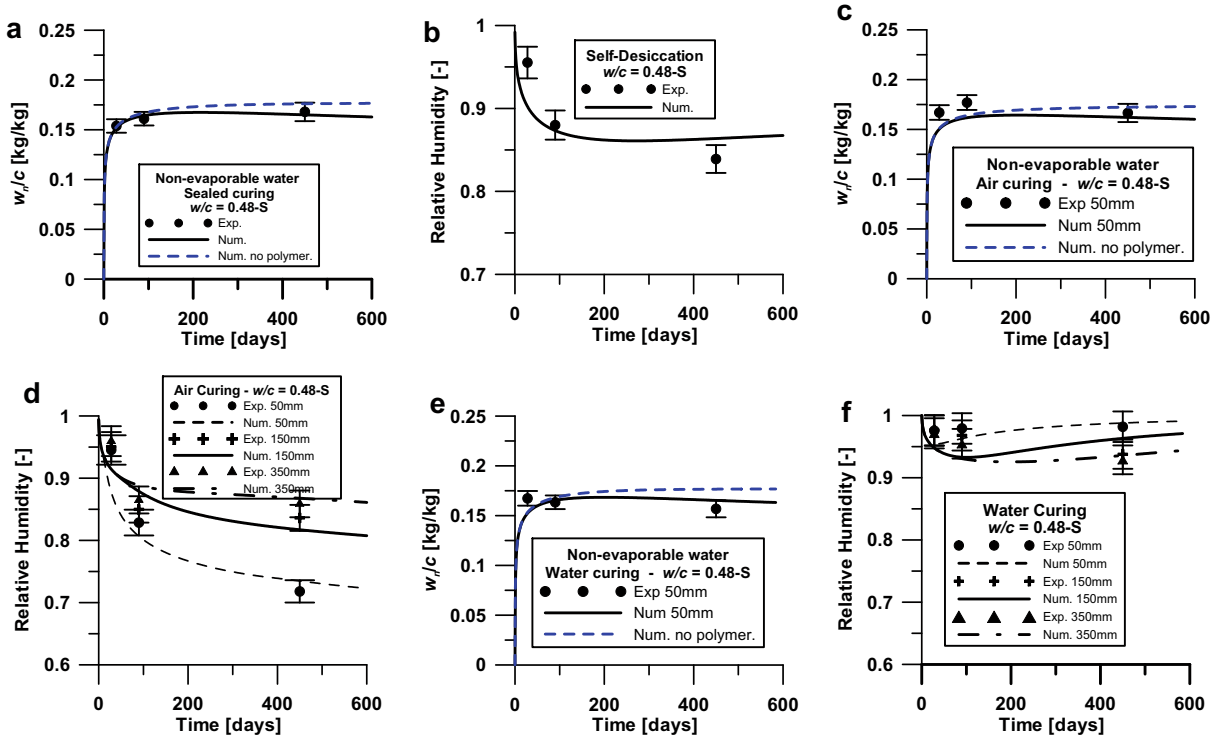


Fig. 22. Data by Persson [10,18,19], concrete Mix 8: non-evaporable water and relative humidity under sealed conditions (a, b), air curing (c, d), and water curing (e, f).

air curing (drying). During drying the reduction of relative humidity is due to both release of water in the environment and self-desiccation. Both the experimental data and the numerical results show that the overall relative humidity reduction during drying increases for decreasing water-to-cement ratio. This is a direct consequence of the self-desiccation process which is more pronounced for low values of water-to-cement ratio. Low values of water-to-cement ratio also influence the gradient of the humidity profile, which tends to be more uniform along the specimen radius. This is particularly true in presence of silica fume. At 450 days, the relative humidity gradient between points at 50 mm and 350 mm from the exposed surface is less than 0.05 for Mix 5 (low w/c and silica fume) whereas is almost 0.2 for Mix 8 (high w/c and silica fume).

Finally, sub-figures f in Figs. 19–22 show the evolution of relative humidity at three different locations in specimens subjected to water curing (wetting). The relative humidity initially decreases at all locations as a consequence of self-desiccation. Later, the water supplied from the environment is not completely consumed by the chemical reaction and the relative humidity increases again. This phenomenon (wetting) is, of course, faster at points located close to the external boundaries. It must be noted here, that in this case the agreement between the experimental data and the numerical results is not as good as in the other cases, even if it can be still considered satisfactory. The reduced accuracy of the numerical predictions in the case of wetting could depend by the fact that: (1) the model does not distinguish between the adsorption isotherm and desorption isotherm and (2) sorption/desorption isotherms have been calibrated on the basis of desorption data. This point certainly requires further investigation and future research.

11. Conclusions

In this paper the model presented in Part I of this study [1] has been calibrated and validated by an extensive analysis of experi-

mental data available in the literature. Based on the obtained results it is possible to draw the following conclusions:

1. The present formulation can simulate correctly and predict with great accuracy the evolution of cement hydration and silica fume (pozzolanic) reaction for concrete mixes characterized by a wide range of water-to-cement ratio and low silica fume content. This is achieved by the formulation of evolution laws for the hydration degree and for the silica fume reaction degree.
2. For high silica fume content mixes, rarely used in practise, experimental data are not available in the literature and further research is needed to verify the applicability of the present model to these cases.
3. The correct simulation of the effect of hydration and pozzolanic reaction allows an accurate simulation of the phenomena that characterize early age behavior of standard and high-performance concrete mixes, such as self-desiccation and self-heating. This capability is an essential prerequisite to simulate early age cracking in massive structures (e.g. dams), where the heat released by the chemical reactions may be significant, and high-performance structures (e.g. bridge decks), where shrinkage induced by self-desiccation cannot be neglected.
4. In addition to early age self-desiccation data, the present model can simulate medium- and long-term increase of free (evaporable) water and relative humidity under sealed conditions, as shown by some experimental data relevant to concrete mixes containing silica fume [10]. This is achieved by: (a) assuming that this phenomenon is caused by silicate polymerization (which is known to release some of the chemically bound water) and (b) modeling polymerization through an evolution law for the silicate polymer concentration. The present model is able to reproduce the existing experimental data that features the effect of polymerization. Nevertheless, due to the fact that polymerization data is scarce in the literature, additional calibration and validation is certainly needed for this component of the model.

5. Finally, the model can simulate and predict with unprecedented accuracy drying experimental data for a wide range of standard and high-performance concrete mixes, with and without silica fume.

Since hydration degree and silica fume reaction degree provide the extent of concrete aging, the same theory can be used to simulate the early age effects on strength (strength build-up), nonlinear mechanical behavior, and fracturing. This subject is part of an ongoing research effort by the authors.

Acknowledgement

The first author gratefully acknowledges the financial support of CTG (Italcementi Group) through the CIS-E Consortium.

Appendix A

For a three-node triangular element the shape functions can be expressed as $N_i(r, z) = 0.5(a_i + b_i r + c_i z)/\Omega^e$ ($i = 1, \dots, 3$), where r = radial coordinate, z = longitudinal coordinate, and Ω^e = element area [2]. Consequently, one has $\partial N_i/\partial r = 0.5b_i/\Omega$, and $\partial N_i/\partial z = 0.5c_i/\Omega$. By using the previous expressions and by solving the integrals in Eqs. (5)–(7) with a one-point gauss formula, one obtains

$$\mathbf{K}_1^{ele} = \frac{\bar{C}_1 \Omega^e}{12} \mathbf{A}; \quad \mathbf{K}_2^{ele} = -\frac{\bar{D}_h}{4\Omega^e} \mathbf{B}^{ele}; \quad \mathbf{F}_1^{ele} = \frac{\bar{C}_2 \Omega^e}{3} \mathbf{I} \quad (11)$$

$$\mathbf{K}_3^{ele} = \frac{\bar{C}_3 \Omega^e}{12} \mathbf{A}; \quad \mathbf{K}_4^{ele} = -\frac{\bar{\lambda}}{4\Omega^e} \mathbf{B}^{ele}; \quad \mathbf{F}_2^{ele} = \frac{\bar{C}_4 \Omega^e}{3} \mathbf{I} \quad (12)$$

$$\mathbf{A} = \begin{bmatrix} 2 & 1 & 1 \\ 1 & 2 & 1 \\ 1 & 1 & 2 \end{bmatrix} \quad \mathbf{I} = \begin{bmatrix} 1 \\ 1 \\ 1 \end{bmatrix} \quad (13)$$

$$\mathbf{B}^{ele} = \begin{bmatrix} b_1^2 + c_1^2 + \delta_1 & b_1 b_2 + c_1 c_2 + \delta_2 & b_1 b_3 + c_1 c_3 + \delta_3 \\ b_1 b_2 + c_1 c_2 + \delta_1 & b_2^2 + c_2^2 + \delta_2 & b_2 b_3 + c_2 c_3 + \delta_3 \\ b_1 b_3 + c_1 c_3 + \delta_1 & b_2 b_3 + c_2 c_3 + \delta_2 & b_3^2 + c_3^2 + \delta_3 \end{bmatrix} \quad (14)$$

where the overbar means evaluation at the centroid of the element, and $\delta_i = -2b_i\Omega_e/3r$ for axis-symmetric meshes and $\delta_i = 0$ for two-dimensional planar meshes.

References

- [1] Di Luzio G, Cusatis G. Hygro-thermo-chemical modeling of high performance concrete. I: Theory. *Cem Concr Compos*, in press, doi:10.1016/j.cemconcomp.2009.02.015.
- [2] Belytschko T, Liu WK, Moran B. Nonlinear finite elements for continua and structures. New York: John Wiley and Sons; 2000.
- [3] Bažant ZP, Najjar LJ. Nonlinear water diffusion in nonsaturated concrete. *Mater Struct* 1972;5(25):3–20.
- [4] Pantazopoulou SJ, Mills RH. Microstructural aspects of the mechanical response of plain concrete. *ACI Mater J* 1995;92(6):605–16.
- [5] Norling Mjönell K. A model on self-desiccation in high-performance concrete. In: Self-desiccation and its importance in concrete technology, proceedings of the international research seminar, Lund, Sweden; 1997. p. 141–57.
- [6] Cervera M, Oliver J, Prato T. Thermo-chemical-mechanical model for concrete. I: hydration and aging. *J Eng Mech, ASCE* 1999;125(9):1018–27.
- [7] de Schutter G, Taerwe L. General hydration model for portland cement and blast furnace slag cement. *Cem Concr Res* 1995;25:593–604.
- [8] Xi Y, Bažant ZP, Jennings HM. Moisture diffusion in cementitious materials – moisture capacity and diffusivity. *Adv Cem Based Mater* 1994;1:258–66.
- [9] Taylor HFW. Cement chemistry. Telford (London): Thomas; 1997.
- [10] Persson B. Hydration and strength of high performance concrete. *Adv Cem Based Mater* 1996;3:107–23.
- [11] Xi Y, Bažant ZP, Jennings HM. Moisture diffusion in cementitious materials – adsorption isotherms. *Adv Cem Based Mater* 1994;1:258–66.
- [12] Baroghel-Bouny V, Mainguy M, Lassabatere T, Coussy O. Characterization and identification of equilibrium and transfer moisture properties for ordinary and high-performance cementitious materials. *Cem Concr Res* 1999;29:1225–38.
- [13] Pane I, Hansen W. Investigation of blended cement hydration by isothermal calorimetry and thermal analysis. *Cem Concr Res* 2005;35:1155–64.
- [14] Bentz DP, Waller V, De Larrard F. Prediction of adiabatic temperature rise in conventional and high-performance concretes using a 3-D microstructural model. *Cem Concr Res* 1998;28(2):285–97.
- [15] Lura P, Jensen OM, van Breugel K. Autogenous shrinkage in high-performance cement paste: an evaluation of basic mechanisms. *Cem Concr Res* 2003;33:223–32.
- [16] Ayano T, Wittmann FH. Drying, moisture distribution, and shrinkage of cement based materials. *Mater Struct* 2002;35:134–40.
- [17] Kim J-K, Lee C-S. Moisture diffusion of concrete considering self-desiccation at early age. *Cem Concr Res* 1999;29:1921–7.
- [18] Persson B. Moisture in concrete subjected to different kinds of curing. *Mater Struct* 1997;30:533–44.
- [19] Persson B. Seven-year study on the effect of silica fume in concrete. *Adv Cem Based Mater* 1998;7:139–55.
- [20] Neville AM. Properties of concrete. New York: John Wiley and Sons; 1997.
- [21] Bažant ZP, Kaplan MF. Concrete at high temperatures: material properties and mathematical models. London: Longman (Addison-Wesley); 1996.
- [22] Mindess S, Young JF. Concrete. Englewood Cliffs, NJ: Prentice-Hall; 1981.
- [23] Waller V, de Larrard F, Roussel P. Modelling the temperature rise in massive HPC structures. In: 4th international symposium on utilization of high-strength/high-performance concrete, RILEM; May 1996. p. 415–21.
- [24] Brough AR, Dobson CM, Richardson IG, Groves GW. In situ solid-state NMR studies of Ca_3SiO_5 : hydration at room temperature and at elevated temperatures using ^{29}Si enrichment. *J Mater Sci* 1994;29:3926–40.